HHS Public Access

Author manuscript

Med Eng Phys. Author manuscript; available in PMC 2021 September 01.

Published in final edited form as:

Med Eng Phys. 2020 September ; 83: 64–72. doi:10.1016/j.medengphy.2020.07.011.

Compartmental Force and Contact Location Sensing in Instrumented Total Knee Replacements

Mohsen Safaei[a], **R. Michael Meneghini**[b], **Steven R. Anton**[a,*]

[a]Department of Mechanical Engineering, Tennessee Technological University, Cookeville, TN 38505 USA,

[b]Department of Orthopaedic Surgery, Indiana University School of Medicine, Indianapolis, IN 46202 USA,

Abstract

For the past three decades, total knee replacement has become the main solution for progressed knee injuries and diseases. Due to a lack of postoperative in vivo data, a universal correlation between intra- and postoperative soft tissue balance in the knee joint has not been established. In this work, an instrumented knee implant design with six piezoelectric transducers embedded in the tibial bearing is proposed. The aim of the presented device is to measure the total and compartmental forces as well as to track the location of contact points on the medial and lateral compartments of the bearing. A numerical analysis using finite element software is first performed to obtain the best sensory system arrangement inside the bearing. The chosen design is then used to fabricate a prototype of the device. Several experiments are designed and performed using the prototype, and the ability of the proposed system to track the location and magnitude of applied compartmental forces on the bearing is evaluated. The experimental results show that the instrumented knee bearing is able to accurately measure the compartmental force quantities with a maximum error of 2.6% of the peak axial load, and the CP locations with a maximum error of less than 1 mm.

Keywords

Total knee replacement; piezoelectric sensing; integrated sensors; orthopedic implant; biomedical sensors

*Corresponding author, santon@tntech.edu.

DECLARATION OF COMPETING INTERESTS

We wish to confirm that there are no known conflicts of interest associated with this work that could have influenced its outcome.

No ethical approval was required for this work.

1. INTRODUCTION

Total knee replacement (TKR) is the main suggestion for people who suffer from end-stage osteoarthritis of the knee. For reference, the components of a TKR are schematically shown in Figure 1(a). Despite the excellent survivorship rate of knee replacements, it has been reported that about 14% of patients are unhappy with the outcomes of their surgery [1]. While many of the reasons for TKR failure have been addressed during the past two decades, instability has been a consistent cause of revision knee surgeries all around the world [2–4]. Instability of the knee joint after surgery can not only cause patient discomfort, it is one of the main reasons for early and late knee failure (less than and more than two years following the operation, respectively) [4]. Instability can be attributed to ligamentous imbalance and misalignment, gap mismatch, and injury to the collateral ligaments [5].

Currently, soft tissue balancing relies on subjective tactile feedback of the surgeon achieved via ligamentous tensioning [6]. Stiffness and instability are common signs of knee replacement failure or dysfunction, and they are directly dependent on soft tissue balancing, showing that traditional subjective balancing techniques during knee replacement are suboptimal [7]. Computer assisted alignment techniques developed in recent years, however, have improved intraoperative balance of the joint by providing surgeons with medial and lateral force data, and, as a result, more accurate soft tissue balance and bone cut measurements [8–11]. Despite the numerous efforts performed to correlate intraoperatively obtained data and postoperative function of the joint, the establishment of a comprehensive correlation has not been accomplished mostly due to lack of sufficient correlation of intraoperative force measurements to in vivo loads experienced by patients after surgery [12]. Computational modeling has also been suggested as an effective tool to provide insights that cannot easily be achieved experimentally. Current modeling techniques are able to simulate articular surface interactions to a large extent, but the postoperative interactions between articular geometry, passive ligaments, and muscles are not well defined [13].

In order to obviate the current limitations, several researchers have suggested various designs of instrumented knee implant systems with the ability to collect in vivo data and monitor the internal joint interactions. Amongst these instrumented TKR devices, two groups have used their implant in actual preclinical trials in the human body [15]. D’Lima et al. in 2005 [16], and Heinlein et al. in 2007 [17], proposed and tested these sensorized knee implants. Both designs employed several strain gauges in the tibial tray stem along with data collection and transmission electronics and a magnetic coil to receive required power from an external magnetic source placed around the patient’s knee [17–20]. Another instrumented TKR design was proposed by Crescini et al. in 2009 [21–23] utilizing six magnetoresistive sensors inside the tibial bearing to measure axial forces applied on the bearing, and magnetic induction to power the embedded system. While the abovementioned devices could successfully provide force sensing capability, the external power requirement of these systems limits their application.

The application of electromagnetic and piezoelectric generators has been suggested to obviate the power requirement limitation of previous devices [24–26]. A piezoelectric knee implant design was presented by Almouahed et al. in 2011 [27]. The same group in 2016

presented an improved prototype of the device that was shown to be able to detect the location of center of pressure (CoP) and measure the total force applied on the bearing surface, and to harvest power from internal knee forces [28]. In another study, a piezoelectric harvester was also utilized by Holmberg et al. in 2013 [29] in the implant tibial stem to power a capacitive sensory system designed to measure the total tibiofemoral force. Ibrahim et al. in 2019 [30] suggested a conceptual design of an instrumented knee implant with a triboelectric transducer to perform simultaneous force sensing and energy harvesting under body loads.

Previously, the authors demonstrated that by using four piezoelectric sensors embedded in the ultra-high molecular weight polyethylene (UHMWPE) bearing, the location of CoP and the total force applied on the bearing can be measured [31]. In addition, the ability of the embedded piezoelectric transducers in generating sufficient power for the data acquisition and transmission electronics was shown through a series of experiments [32]. Moreover, it was demonstrated that piezoelectric discs attached to the tibial tray of the TKR are able to monitor the health of the implant by detecting loosening occurring on the interface of the tray and bone [33]. This work extends the author's previous work by presenting a TKR bearing design equipped with six piezoelectric transducers, as shown in Figure 1(b). The piezoelectric elements are embedded in the bearing to minimize modifications to the original implant geometry. Utilizing six transducers, the device is able to accurately sense compartmental forces and location of contact points (CPs). First, finite element simulation is used to determine an instrumented bearing design with the best sensing performance. A fabricated prototype utilizing the selected design is then used to experimentally evaluate the sensing performance of the system. The aim of this study is to demonstrate that the proposed sensory system design is able to provide compartmental force and CP location sensing, and to establish a numerical and experimental platform that can be used to adapt such a design to various TKR architectures. The eventual goal of this work is to develop an instrumented TKR capable of measuring compartmental forces and CP locations, harvesting energy to power future embedded data processing and wireless data transmission electronics, and monitoring the health of the implant throughout its entire life.

2. INSTRUMENTED IMPLANT DESIGN

The piezoelectric knee bearing introduced in this work intends to measure the compartmental forces and contact point locations on the medial and lateral compartments of the bearing. The design incorporates six piezoelectric transducers placed on the bottom surface of the bearing, where three transducers are placed in each compartment in a symmetrical pattern in order to measure medial and lateral force quantities independently. Note, the sensor arrangement selected in this study is for the specific geometry of the current bearing under investigation. Selection of the best sensor arrangements for other bearing designs needs to be repeated according to the procedure described herein. Figure 1(b) shows a schematic of the proposed instrumented bearing. Axial knee force, as the major contributing force component in the knee joint, is considered as the active force on the bearing in this study. Compression force is applied through the femoral component on both compartments of the bearing. As a result, two axial force components act on the two articulating surfaces of the bearing. By applying compressive force on the bearing, each

piezoelectric sensor measures a portion of the applied force. The three piezoelectrics placed in the medial compartment measure the medial force component, while the three piezoelectrics placed in the lateral compartment measure the lateral force component. The goal is to achieve fully decoupled sensing performance of each group of sensors in order to accomplish accurate compartmental force and CP sensing.

3. FINITE ELEMENT SIMULATION

The first step in developing a sensory system with decoupled medial and lateral compartmental sensing performance is to obtain the best transducer arrangement within the bearing to measure the forces and contain point locations acting on the joint. Thus, a series of finite element simulations in ANSYS (ANSYS Inc.) are performed in which the transducer location is varied, and the sensing ability of the system is evaluated for each arrangement. The capability of the device to measure the total force, compartmental forces, and contact point locations is investigated in the FE analyses.

3.1. SIMULATION SETUP

The FE model of the implant system is shown in Figure 2(a). An actual knee replacement unit is 3D scanned to obtain the CAD geometry of the knee replacement components, and the bearing geometry used in the FE model is modified to include six 4.7 mm diameter, 2 mm deep voids in the bottom surface in order to incorporate the piezoelectric transducers. The piezoelectric sensors are APC 850 (PZT-5A) monolithic PZT discs (APC International Ltd.) with 3.4 mm height and 4.7 mm diameter. Polylactic acid (PLA) is chosen as the material for the bearing, which is the same material used later in prototype fabrication via 3D printing (see Sec. 4.1). The material properties of PZT and PLA are listed in Table 1. Pockets shallower than the piezoelectric elements allow full force transmission to the sensors, thereby maximizing sensing performance of the system [34]. The tibial bearing and femoral component are modeled with SOLID187 elements, the piezoelectrics are modeled with SOLID227 elements, and the contact surfaces are meshed with CONT174 and TARGE174 elements, with a total number of 251,584 nodes and 159,286 elements. A friction coefficient of 0.12 is applied to the interacting surfaces of the femoral component, bearing, and piezoelectrics [35]. A maximum element aspect ratio of 4.7 is achieved by a fine mesh, and convergence of the stress results is accomplished via a mesh refinement study.

In order to select the best arrangement of PZTs inside the bearing, three angular parameters are defined, as shown in Figure 2(b). Angular parameters α_1, α_2, and α_3 specify the location of PZT1, PZT2, and PZT3, respectively. The parameter α_1 is allowed to adopt values of 65°, 100°, and 135°; the parameter α_2 is allowed to adopt values of 60°, 90°, and 120°; and the parameter α_3 is allowed to adopt values of 15°, 30°, and 45°. In total, fifteen different arrangements of piezoelectric sensors are investigated, as listed in Table 2. The bottom surfaces of the PZTs are fixed in the y-direction. Initially, the femoral component and bearing are center-aligned with respect to the geometrical centers of the components. An axial compression force is applied to the femoral component in the y-direction (coordinate

system shown in Figure 2(b)) based on a realistic force profile (shown later in Figure 7) obtained using OpenSim and justified in the authors' previous work [32].

The reaction force generated on each PZT due to the applied femoral force, the pressure distribution on the upper conforming bearing surface, and the contact forces on the medial and lateral bearing compartments are measured for each simulation. The simulations are performed with a timestep of 0.01 sec and 120 steps to form a 1.2 sec timespan of a single gait cycle. The sensing performance of the system is evaluated by comparing the true total, medial, and lateral force, and contact point location quantities with the corresponding quantities measured by the PZT transducers. The true forces and location of CPs are probed in ANSYS. On the other hand, the total, medial, and lateral forces measured by the PZTs can be calculated by summing the individual forces measured by PZTs 1–6, PZTs 1–3, and PZTs 4–6, respectively. The location of CPs on the medial and lateral bearing compartments can be obtained using the equilibrium of moments as presented by:

$$x_{CP} = \sum_{i=1}^{3} x_i F_i / \sum_{i=1}^{3} F_i,\ z_{CP} = \sum_{i=1}^{3} z_i F_i / \sum_{i=1}^{3} F_i,\ \text{on medial compartment}, \tag{1}$$

$$x_{CP} = \sum_{i=4}^{6} x_i F_i / \sum_{i=4}^{6} F_i,\ z_{CP} = \sum_{i=4}^{6} z_i F_i / \sum_{i=4}^{6} F_i,\ \text{on lateral compartment}, \tag{2}$$

where x_{CP} and z_{CP} are the coordinates of the location of CP on each compartment, and x_i and z_i are the coordinates of the ith PZT.

3.2. SIMULATION RESULTS

Figure 3(a) shows the maximum error in measured total, medial, and lateral forces by the PZT sensors for the fifteen different sensor arrangements. Error data are calculated by dividing the forces measured by the PZTs by the true force magnitudes probed in ANSYS at each timestep, and the maximum quantities over one cycle are reported. In addition to force results, the deviation of CP locations measured by the piezoelectric elements from the true locations are presented in Figure 3(b). Note, due to the application of an axial force, the location of CPs does not change during the loading cycle. Considering the results, the optimum sensing performance of the piezoelectric system is achieved in Simulation 5, in which α_1=100°, α_2=120°, and α_3=30° (shown in Figure 4). The zero error in total measured force for each simulation shows that the FE model is converged. An error of 1.4% in measured compartmental forces is achieved for Simulation 5, and the deviation in measured locations of CPs on the medial and lateral compartments is around 0.7 mm. Thus, the sensor arrangement of Simulation 5 is selected as the optimum configuration and used in the next section to perform experimental tests.

4. EXPERIMENTATION

The selected bearing design, shown in Figure 4, is used for fabrication of a prototype instrumented bearing. In order to conduct controlled experiments on the fabricated prototype, several auxiliary components are also designed and fabricated.

4.1. FABRICATION

Figure 5(a) shows an exploded view of the components used in the experiments. The prototype and auxiliary parts are fabricated via 3D printing using a LulzBot TAZ 6 printer (Aleph Objects, Inc.). The fabricated prototype components are shown in Figure 5(b–e). From the bottom view of the bearing in Figure 5(c), it can be seen that several pieces of copper tape are used to provide electrical connection to the top electrodes of the PZTs. The bottom electrodes of the PZTs are connected to the six posts on the bottom plate via several pieces of copper tape, as shown in Figure 5(d).

4.2. TEST SETUP

The instrumented knee bearing system is placed in an experimental test setup in order to evaluate the sensing ability of the system. The test setup consists of an MTS-810 load frame (MTS Systems Corp.), the instrumented implant system, sensing circuitry, and a data acquisition system, as shown in Figure 6(a). The load frame provides the desired compression force during the experiments. A close-up view of the instrumented implant system is shown in Figure 6(b). An adjustable fixture is placed under the knee bearing which provides movement of the bearing in two perpendicular directions with the help of several adjustment screws on the four sides of the fixture. A customized fixture is fabricated to hold the femoral component in a fixed position during the tests. Pressure sensitive film (Prescale medium-range pressure sensitive film; Fujifilm Corp.) is inserted between the femoral component and the instrumented bearing to record the actual location of contact areas. The sensory circuit is composed of six 500 kΩ resistors, with each resistor connected in parallel to a single PZT sensor. A schematic of the sensory circuit for each piezoelectric transducer is shown in Figure 6(c).

Two distinct sets of experiments are designed to investigate the ability of the instrumented knee bearing to track the CP locations and the compartmental force magnitudes for various placements of the femoral component relative to the bearing. Each set consists of several tests in which the femoral component is held at a fixed position and the bearing is moved. The initial alignment of the bearing and femoral component is achieved visually on an arbitrary center position for each set of tests. This position is considered as the origin with relative locations of the bearing and femoral component of x=0 and z=0. Note, the directions of movement achieved by the fixture are shown in Figure 6(b). Experiment set 1 includes eight different positions of the bearing along the x-direction (Test 1–8), and experiment set 2 includes 8 different positions of the bearing along the z-direction (Test 9–16). The femoral component is aligned on the most lateral position in Test 1 and on the most medial position in Test 8. On the other hand, the femoral component is located on the most posterior position in Test 9 and on the most anterior position in Test 16. The medial, lateral, anterior, and posterior directions are shown in Figure 1(a) for reference. The knee bearing is moved by 1 mm increments in each direction to achieve the relative positions. The relative positions of the bearing and femoral components are listed in Table 3 for all tests.

A compression force profile representing realistic axial knee loading (same profile used for FE simulations) is applied to the instrumented bearing using the femoral component. Since the load frame is not able to exactly follow the command force, the true load applied through

the femoral component is obtained from the built-in load cell of the load frame at a sampling frequency of 1000 Hz and with a resolution of 5 mN. As a result of the applied load, the piezoelectric transducers generate voltage signals proportional to their respective reaction force. The voltage signals are collected across all the load resistances via a LabVIEW (National Instrument Corp.) program. Next, the measured voltages are imported into MATLAB and post-processed in order to obtain measured compartmental forces and CP locations. In addition, an image processing code is written in MATLAB to quantify the true location of the CPs from the pressure sensitive film results with an accuracy of 0.09 mm. First, the following governing electromechanical differential equation representing a piezoelectric transducer connected in parallel to a resistive load, R, subject to a low frequency compressive force, $F(t)$, is utilized to calculate individual forces sensed by each piezoelectric from the generated voltage signal, $V(t)$:

$$C_p \frac{dV(t)}{dt} + \frac{V(t)}{R} = d_{33} \frac{dF(t)}{dt}, \tag{3}$$

where d_{33} is the piezoelectric strain coefficient, t is time, and C_p is the capacitance of the piezoelectric disc with a cross-sectional area of A, thickness of h, and dielectric permittivity ε_{33}^{T} of , given as:

$$C_p = \varepsilon_{33}^{T} A / h\,. \tag{4}$$

The individual force quantities measured by the PZTs are then used to calculate the total force and compartmental forces. Finally, the CP locations on each compartment of the bearing are also calculated using Eqs. (1) and (2).

4.1. EXPERIMENTAL RESULTS

Sixteen individual tests are performed according to the procedure described in the previous section. A comparison of the total force measured by the PZTs and the profile obtained from the load frame's buil-tin load cell is presented in Figure 7(a) and (b) for Test 1 and Test 9, respectively. It can be observed that the sensory system successfully measures the total applied force profile with a small amount of error. The small deviations in measured forces from actual input forces is caused by the low signal-to-noise ratio of the voltage signal in these areas, and nonlinear behavior of the piezoelectric d_{33} coefficient [32].

A similar comparison is performed for each test, and the error in the measured maximum total force compared to the actual forces is calculated. Figure 8(a) and (b) show the calculated error for Tests 1–8 and Tests 9–16, respectively. It can be seen that the maximum error at peak axial force (62 N) is less than 2.6 % of the total force for all tests, thus showing the accuracy of the sensory system. Similar errors in measured forces have been previously reported in the works of Crescini et al. [22] and Heinlein et al. [36]. Thus, it can be concluded that the proposed design of the instrumented TKR is capable of measuring the total axial force acting on the knee joint with a small error within the input range of approximately three times body weight. The ability of the device to measure higher force

levels that may be experienced during activities such as jumping and running should be investigated in the future.

In addition to the total force profile, the compartmental forces are measured by the piezoelectric system. Figure 9(a) and (b) show the calculated medial and lateral compartmental forces, respectively, for Tests 1–8. It can be seen that when the tests proceed from Test 1 to Test 8, the medial force increases and the lateral force decreases. Considering the movement of the femoral component in the lateral to medial direction, the abovementioned trend shows the ability of the sensing device to track the changes in compartmental forces. Similarly, the compartmental forces for Tests 9–16 are plotted in Figure 9(c) and (d). The relatively constant force profiles represent the small movement of the bearing in the medial-lateral direction during the tests, which is in conformity with the test procedure defined for Tests 9–16 where the bearing moves in the posterior to anterior direction only.

Figure 10 and Figure 11 show the CP locations measured by the PZTs (white dots in the figure) plotted over an image of the knee bearing for Tests 1–8 and Tests 9–16, respectively. In addition, the true location of contact areas between the femoral component and bearing observed from the pressure sensitive films (red areas) are also plotted on the bearing images, with the center of the contact area specified with a blue star. A summary of the total deviations for each test obtained on both bearing compartments is provided in Table 4. Comparing the measured and true CP locations on both compartments, it can be seen that the PZT sensing system can track the CPs with a maximum deviation of 1.6 mm. D'Lima et al. [16] have previously reported an error of less than 1.5 mm in detecting the location of tibiofemoral axial compression forces. The device was implanted in a patient's knee and used in an in vivo study to measure the location and quantity of forces.

In order to provide a better comparison of the measured and true CP locations, the movement paths of CPs on the bearing compartments are plotted in Figure 12 (a) and (b) for Tests 1–8 and 9–16, respectively. The results show that the piezoelectric sensory system can accurately track the CP locations given relative movement of the femoral component and instrumented bearing in both directions.

5. CONCLUSIONS

This work investigates the sensing performance of an instrumented total knee replacement design with six piezoelectric transducers embedded in the bearing component of the implant. The piezoelectric sensory system is designed to measure the medial and lateral compartmental forces and the location of compartmental contact points (CPs) of the bearing. Initially, several arrangements of piezoelectric sensors are considered and the sensing performance of each arrangement is evaluated numerically through finite element (FE) analysis. The sensory system arrangement with the best performance obtained from FE simulations is then utilized to create a prototype for experimental characterization. A series of experiments are then performed to investigate the sensing ability of the device with regards to compartmental forces and CP locations. Experimental results showed that the device is able to measure the total force with a maximum error of 2.6% and the CP locations

with a maximum error of less than 1.6 mm. In addition, the device showed excellent performance in tracking the variation in medial and lateral compartmental forces as well as movement in CP locations when the femoral component was moved relative to the instrumented bearing in both the medial-lateral and anterior-posterior directions. This work has some limitations and future work will attempt to address them. The performance of the device needs to be evaluated using a knee simulator with the ability to provide various degrees of motion available in the knee joint. This will include flexion-extension and internal-external rotation during the loading cycle, which allows for a wider range of tibiofemoral contact locations than permitted within the limitations of the current experimental setup. The arrangement of sensors proposed in this study is selected based on a specific TKR geometry, however, the arrangement needs to be investigated for other implant designs and materials. In future work, the sensing functionalities of the sensory system will be extended to measure various force and moment components acting on the knee. In addition, fabrication of prototypes using medical-grade UHMWPE, utilizing lead-free piezoelectric transducers, encapsulating the electronics, and using biocompatible packaging need to be considered. The long-term goal of this study is to incorporate the sensing, energy harvesting, and structural health monitoring capabilities of the piezoelectric transducers into an integrated instrumented TKR to provide a self-powered multifunctional knee monitoring system.

ACKNOLEDGEMENTS

Research reported in this publication was supported by the National Institute of Arthritis and Musculoskeletal and Skin Diseases of the National Institutes of Health under Award Number R15AR068663. The content is solely the responsibility of the authors and does not necessarily represent the official views of the National Institutes of Health.

REFERENCES

[1]. Noble PC, Conditt MA, Cook KF, Mathis KB. The John Insall Award: Patient expectations affect satisfaction with total knee arthroplasty. Clinical Orthopaedics and Related Research. 2006;452:35–43. [PubMed: 16967035]

[2]. Sharkey PF, Hozack WJ, Rothman RH, Shastri S, Jacoby SM. Why are total knee arthroplasties failing today? Clinical orthopaedics and related research. 2002;404:7–13.

[3]. Sharkey PF, Lichstein PM, Shen C, Tokarski AT, Parvizi J. Why are total knee arthroplasties failing today—has anything changed after 10 years? J Arthroplasty. 2014;29:1774–8. [PubMed: 25007726]

[4]. Postler A, Lützner C, Beyer F, Tille E, Lützner J. Analysis of Total Knee Arthroplasty revision causes. BMC musculoskeletal disorders. 2018;19:55. [PubMed: 29444666]

[5]. Longo UG, Candela V, Pirato F, Hirschmann MT, Becker R, Denaro V. Midflexion instability in total knee arthroplasty: a systematic review. Knee Surgery, Sports Traumatology, Arthroscopy. 2020:1–11.

[6]. Gustke K The use of smart tibial trials in primary TKA: assuring outcome. Orthopaedic Proceedings. 2018;100:123.

[7]. Anderson C, Golladay G, Roche M, Gustke K, Elson L. Using intraoperative sensors to define intra-articular loading patterns during total knee arthroplasty. Orthopaedic Proceedings. 2018;100:60.

[8]. Roche M, Gustke KA, Law TY. The utilization of smart trials in PCL retaining knees. Semin Arthroplasty. 2015;26:218–28.

[9]. Golladay G, Gustke K, Elson LC, Anderson CR. Intraoperative Sensors for Dynamic Feedback During Soft Tissue Balancing Preliminary Results of a Prospective Multicenter Study| AAOS 2013. 2013.

[10]. Gustke K, Golladay G, Roche M, Jerry G, Elson L, Anderson C. Increased satisfaction after total knee replacement using sensor-guided technology. Bone & Joint Journal. 2014;96:1333–8. [PubMed: 25274917]

[11]. Roche M, Elson L, Anderson C. Dynamic Soft Tissue Balancing in Total Knee Arthroplasty. Orthopedic Clinics of North America. 2014;45:157–65. [PubMed: 24684909]

[12]. Meneghini RM, Ziemba-Davis MM, Lovro LR, Ireland PH, Damer BM. Can Intraoperative Sensors Determine the "Target" Ligament Balance? Early Outcomes in Total Knee Arthroplasty. The Journal of arthroplasty. 2016;31:2181–7. [PubMed: 27155997]

[13]. Rullkoetter PJ, Fitzpatrick CK, Clary CW. How Can We Use Computational Modeling to Improve Total Knee Arthroplasty? Modeling Stability and Mobility in the Implanted Knee. Journal of the American Academy of Orthopaedic Surgeons. 2017;25:S33–S9. [PubMed: 27997412]

[14]. Lum ZC, Shieh AK, Dorr LD. Why total knees fail-A modern perspective review. World journal of orthopedics. 2018;9:60. [PubMed: 29686970]

[15]. Torrão JN, dos Santos MPS, Ferreira JA. Instrumented knee joint implants: innovations and promising concepts. Expert review of medical devices. 2015;12:571–84. [PubMed: 26202322]

[16]. D'Lima DD, Townsend CP, Arms SW, Morris BA, Colwell CW. An implantable telemetry device to measure intra-articular tibial forces. Journal of biomechanics. 2005;38:299–304. [PubMed: 15598457]

[17]. Heinlein B, Kutzner I, Graichen F, Bender A, Rohlmann A, Halder AM, et al. ESB Clinical Biomechanics Award 2008: Complete data of total knee replacement loading for level walking and stair climbing measured in vivo with a follow-up of 6–10 months. Clinical Biomechanics. 2009;24:315–26. [PubMed: 19285767]

[18]. Kirking B, Krevolin J, Townsend C, Colwell CW, D'Lima DD. A multiaxial force-sensing implantable tibial prosthesis. Journal of biomechanics. 2006;39:1744–51. [PubMed: 16023656]

[19]. D'Lima DD, Patil S, Steklov N, Chien S, Colwell CW. In vivo knee moments and shear after total knee arthroplasty. Journal of Biomechanics. 2007;40:S11–S7. [PubMed: 17462659]

[20]. D'Lima D, Fregly B, Colwell C. Implantable sensor technology: measuring bone and joint biomechanics of daily life in vivo. Arthritis research & therapy. 2013;15:203. [PubMed: 23369655]

[21]. Crescini D, Sardini E, Serpelloni M. An autonomous sensor for force measurements in human knee implants. Procedia Chemistry. 2009;1:718–21.

[22]. Crescini D, Sardini E, Serpelloni M. Design and test of an autonomous sensor for force measurements in human knee implants. Sensors and Actuators A: Physical. 2011;166:1–8.

[23]. Gazzoli M, Sardini E, Serpelloni M, Donzella G. Human Knee Prosthesis Equipped with Force Sensors. BIODEVICES2011. p. 349–52.

[24]. Luciano V, Sardini E, Serpelloni M, Baronio G. An energy harvesting converter to power sensorized total human knee prosthesis. Measurement Science and Technology. 2014;25:025702.

[25]. Platt SR, Farritor S, Garvin K, Haider H. The use of piezoelectric ceramics for electric power generation within orthopedic implants. Mechatronics, IEEE/ASME Transactions on. 2005;10:455–61.

[26]. Platt SR, Farritor S, Haider H. On low-frequency electric power generation with PZT ceramics. Mechatronics, IEEE/ASME Transactions on. 2005;10:240–52.

[27]. Almouahed S, Gouriou M, Hamitouche C, Stindel E, Roux C. The use of piezoceramics as electrical energy harvesters within instrumented knee implant during walking. Mechatronics, IEEE/ASME Transactions on. 2011;16:799–807.

[28]. Almouahed S, Hamitouche C, Stindel E. Self-powered device for tibiofemoral force measurement in knee implant. Advanced Technologies for Signal and Image Processing (ATSIP), 2016 2nd International Conference on: IEEE; 2016 p. 359–63.

[29]. Holmberg J, Alexander L, Rajamani R, Bechtold J. Battery-Less Wireless Instrumented Knee Implant. Journal of Medical Devices. 2013;7:011006.

[30]. Ibrahim A, Jain M, Salman E, Willing R, Towfighian S. A smart knee implant using triboelectric energy harvesters. Smart Materials and Structures. 2019;28:025040. [PubMed: 31258261]

[31]. Safaei M, Meneghini RM, Anton SR. Force detection, center of pressure tracking, and energy harvesting from a piezoelectric knee implant. Smart Materials and Structures. 2018;27:114007. [PubMed: 30297976]

[32]. Safaei M, Meneghini RM, Anton SR. Energy Harvesting and Sensing with Embedded Piezoelectric Ceramics in Knee Implants. IEEE/ASME Transactions on Mechatronics. 2018;32:864–74.

[33]. Ponder RI, Safaei M, Anton SR. Validation of Impedance-Based Structural Health Monitoring in a Simulated Biomedical Implant System. ASME 2018 Conference on Smart Materials, Adaptive Structures and Intelligent Systems: American Society of Mechanical Engineers; 2018 p. V002T05A8.

[34]. Safaei M, Meneghini RM, Anton SR. Parametric analysis of electromechanical and fatigue performance of total knee replacement bearing with embedded piezoelectric transducers. Smart Materials and Structures. 2017;26:094002. [PubMed: 29225424]

[35]. Kurtz SM. UHMWPE biomaterials handbook: ultra high molecular weight polyethylene in total joint replacement and medical devices. 3 ed: William Andrew; 2015

[36]. Heinlein B, Graichen F, Bender A, Rohlmann A, Bergmann G. Design, calibration and preclinical testing of an instrumented tibial tray. Journal of biomechanics. 2007;40:4–10.

[37]. Polymaker. PolyLite PLA (formerly PolyPlus PLA). Accessed on: 17 June 2018.

[38]. APC International Ltd. Physical and piezoelectric properties of APC materials. Accessed on: 11 November 2018.

Highlights

- An instrumented knee implant using multiple piezoelectric transducers is proposed
- The aim is to measure the compartmental joint forces and contact point locations
- The device can measure the medial and lateral forces with error less than 2.6%
- The device can track the contact point locations with error less than 1 mm

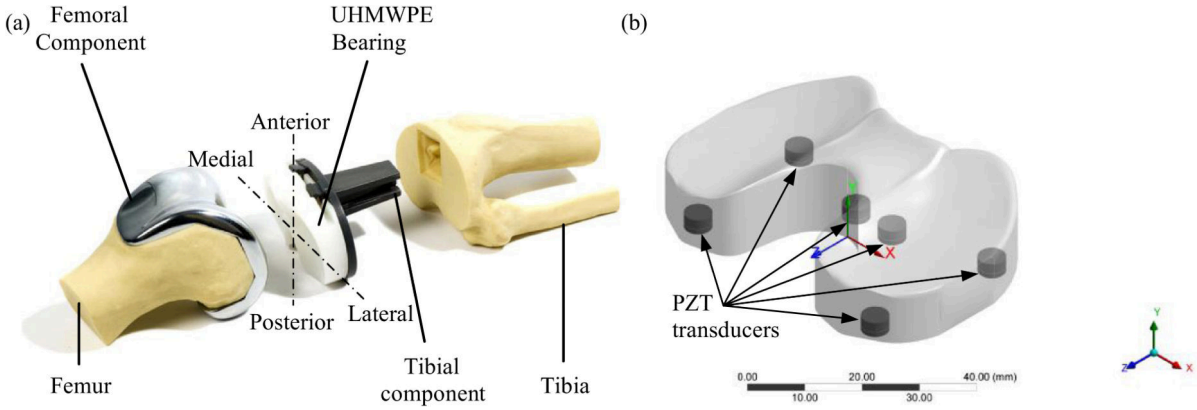

Figure 1.

Schematic of (a) knee replacement components (right knee, image courtesy of http://delcore.org), and (b) knee bearing with six embedded piezoelectric transducers.

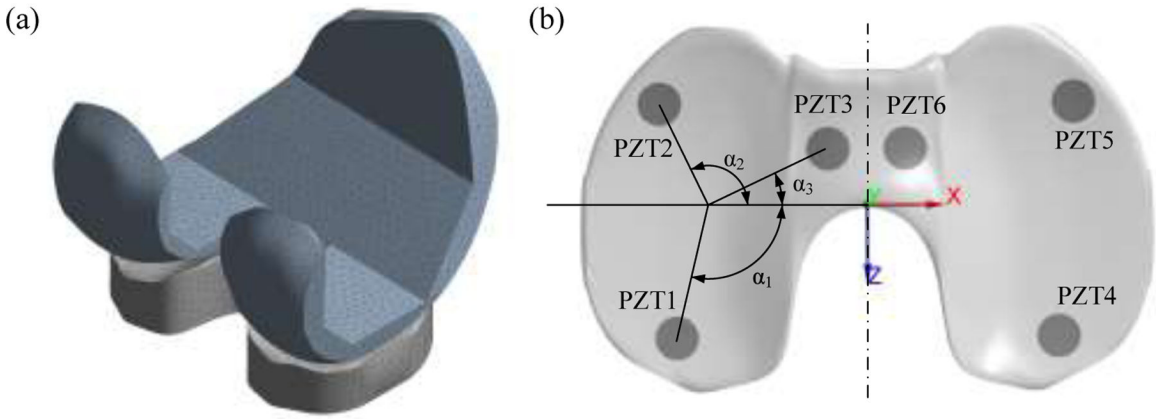

Figure 2.

FE model of knee implant including (a) femoral component and tibial bearing, and (b) schematic representation of angular parameters defined for FE simulation (right knee).

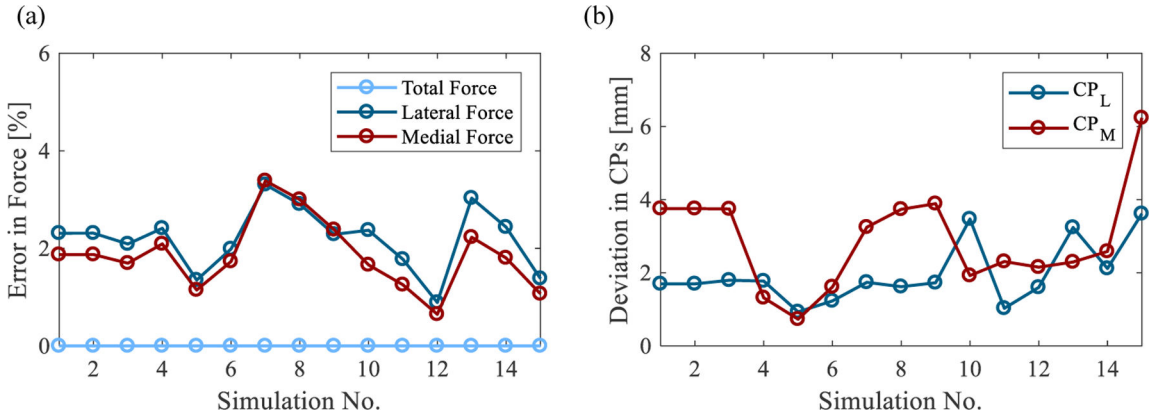

Figure 3.

FE simulation results including (a) error in measured total and compartmental forces, and (b) deviation in measured CP locations.

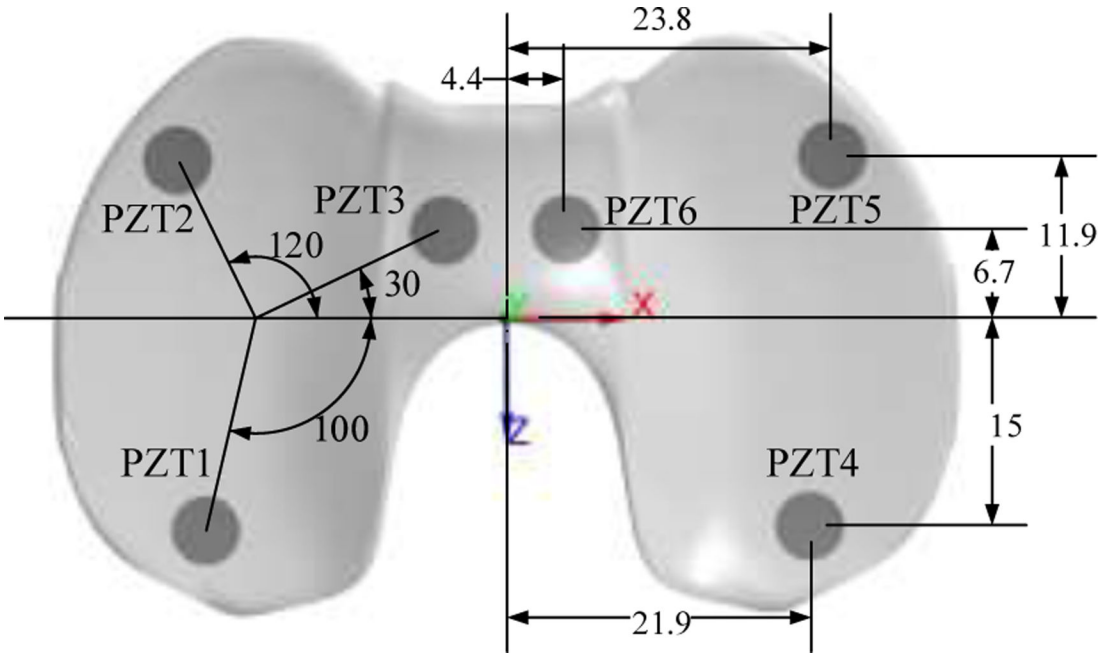

Figure 4.
Optimum arrangement of PZT transducers inside the knee bearing used in Simulation 5.

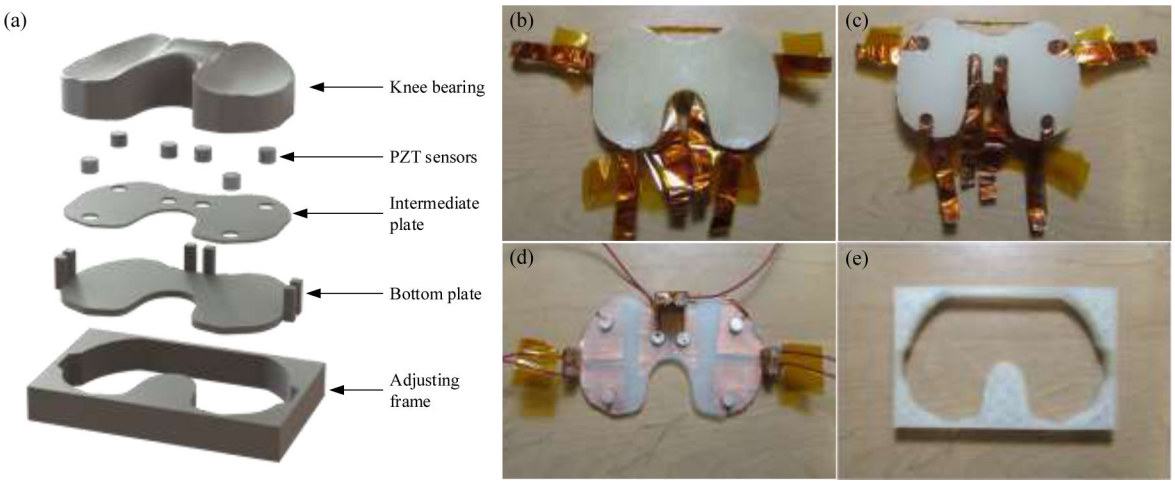

Figure 5.

(a) Exploded view of instrumented bearing and additional parts for experiment; fabricated knee bearing and auxiliary parts showing (b) top view of bearing, (c) bottom view of bearing, (d) PZTs, intermediate, and bottom plates, and (e) adjusting frame.

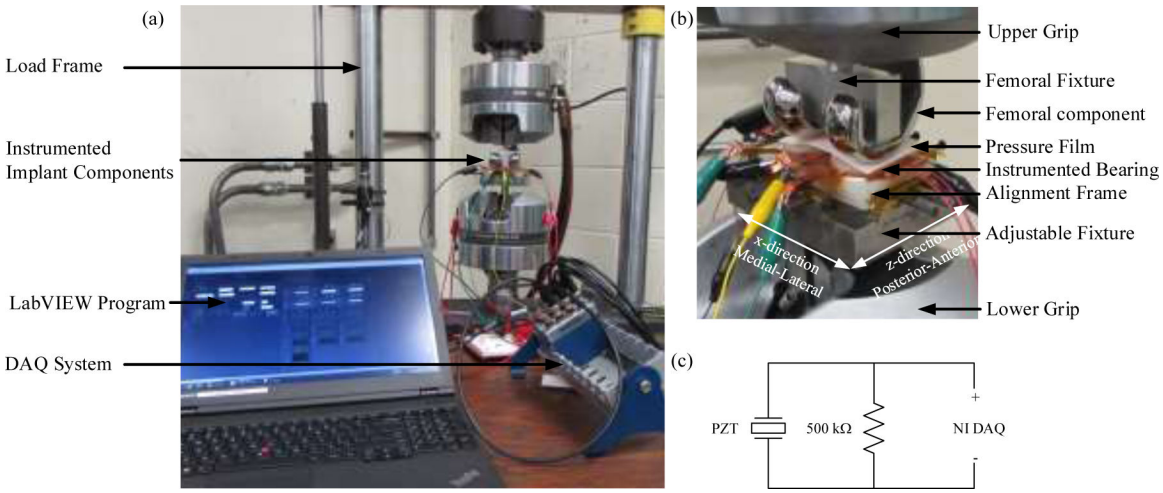

Figure 6.

Experimental test setup showing (a) overall setup, (b) close-up view of femoral component and instrumented bearing system, and (c) schematic of piezoelectric sensing circuitry.

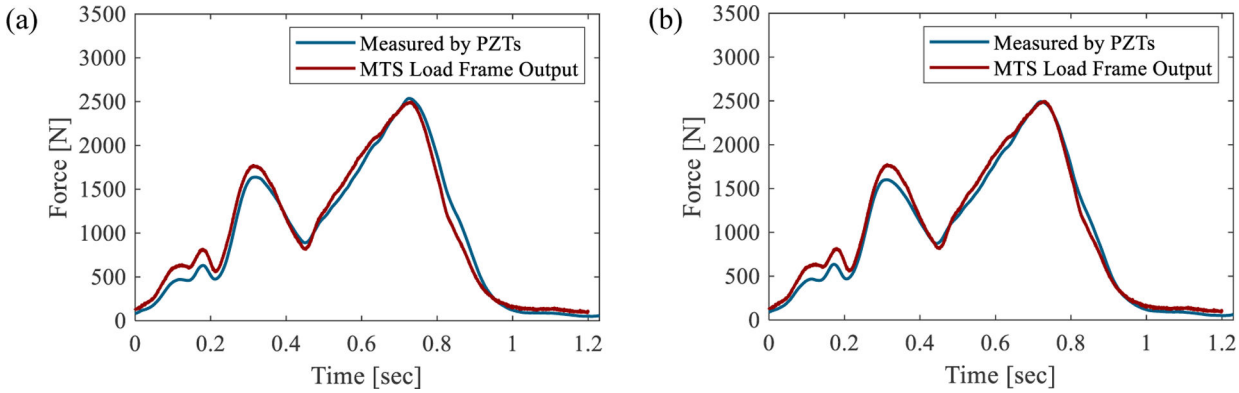

Figure 7.

Comparison of total force on the bearing measured by PZTs and recorded by load frame for (a) Test 1, and (b) Test 9.

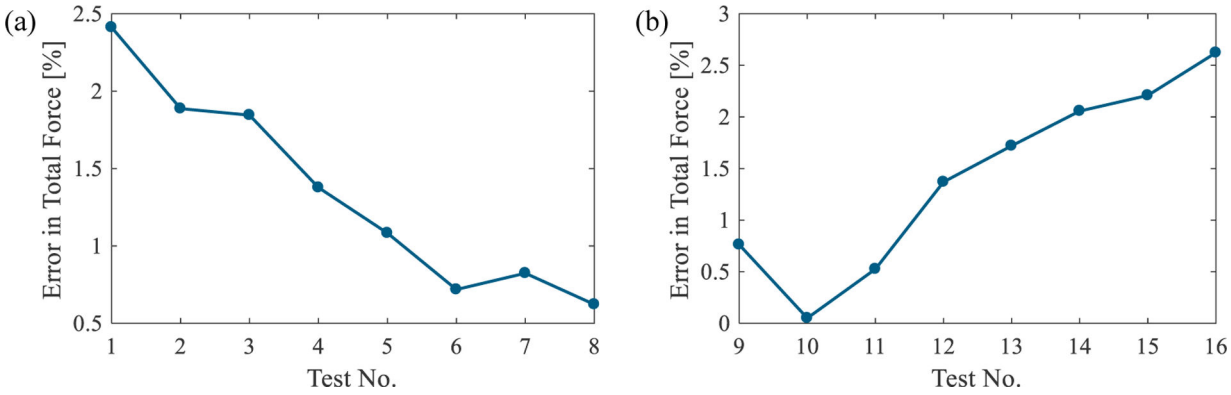

Figure 8.

Calculated error in measured total force from actual values for (a) Tests 1–8, and (b) Tests 9–16.

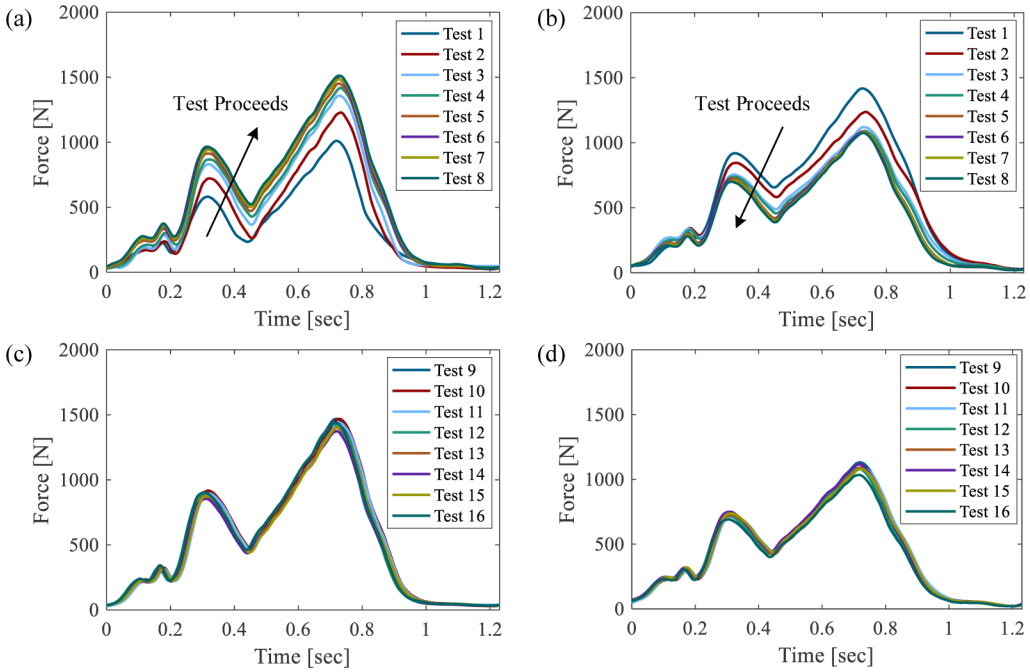

Figure 9.

Measured compartmental force profiles including (a) medial and (b) lateral force for Tests 1–8, and (c) medial and (d) lateral force for Tests 9–16.

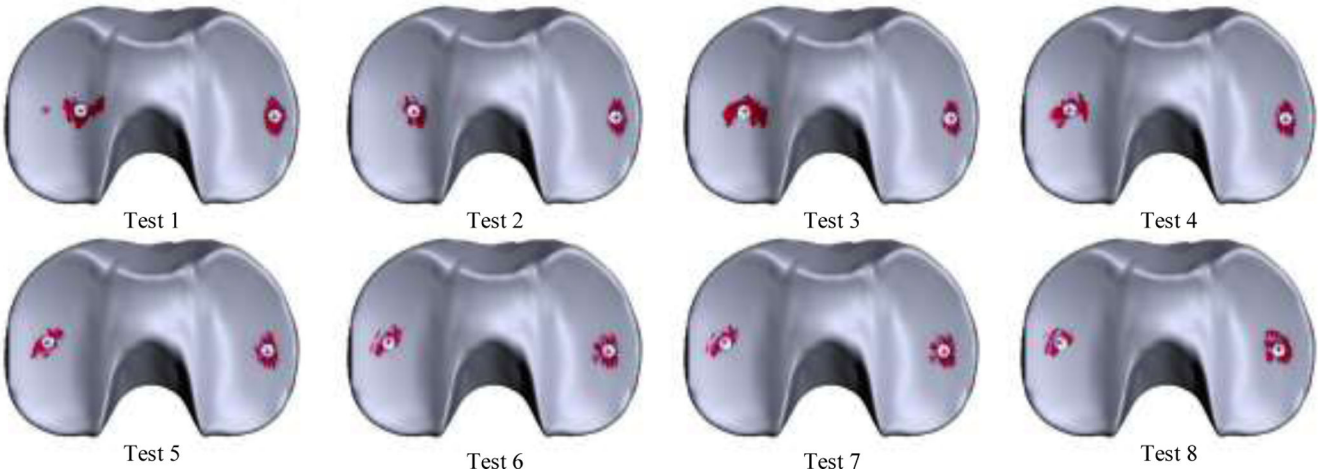

Figure 10.

Measured CP locations using PZTs (white circles) and true contact areas recorded by pressure films (red areas; blue stars represent center of contact area) overlaid on an image of knee bearing for Tests 1–8.

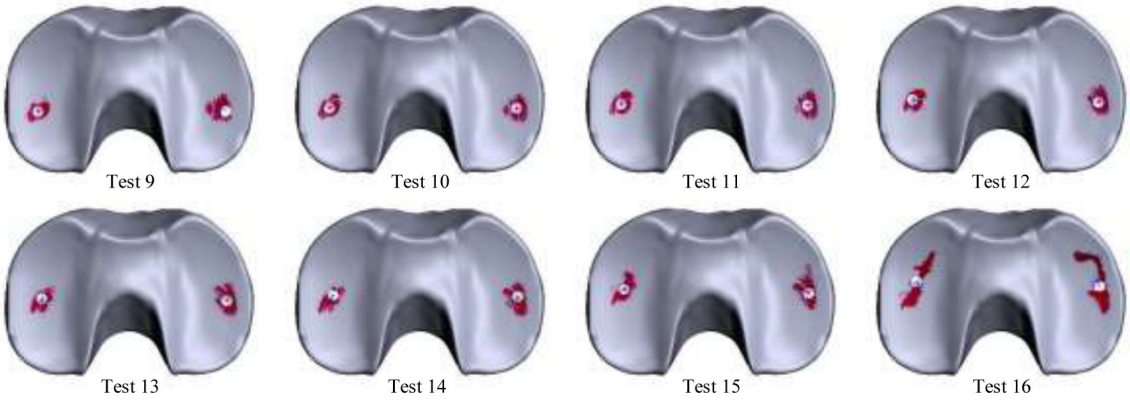

Figure 11.

Measured CP locations using PZTs (white circles) and true contact areas recorded by pressure films (red areas; blue stars represent center of contact area) overlaid on an image of knee bearing for Tests 9–16.

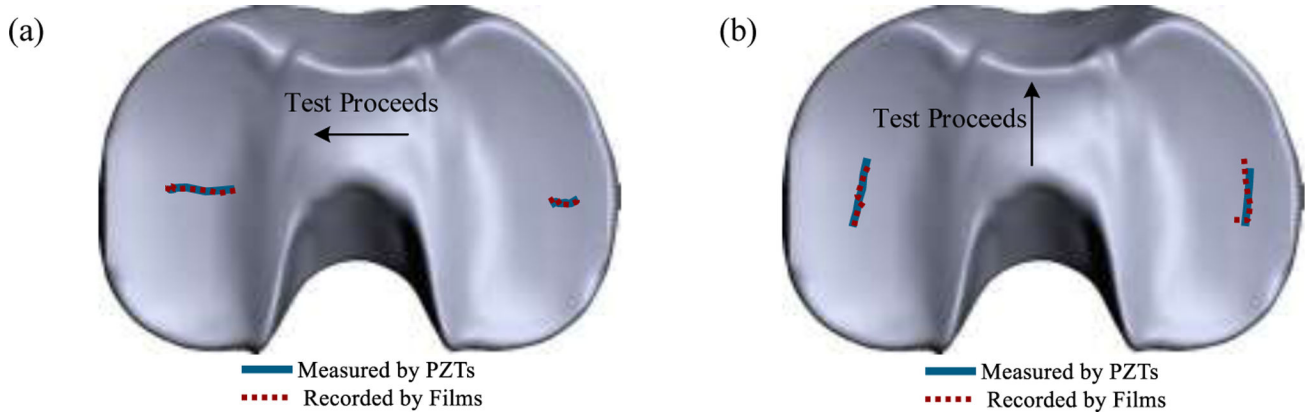

Figure 12.

Movement path of CPs measured by PZTs and recorded by pressure sensitive films for (a) Tests 1–8, and (b) Tests 9–16.

Table 1.

Material properties for PLA and piezoelectric transducer (ε_0 = 8.854×10^{-12} F/m)

Material Properties	PLA Bearing [37]	APC 850 (PZT-5A) Piezoelectric [38]
Young's Modulus [GPa]	3.5	54
Poisson's Ratio	0.42	0.35
Density [kg/m^3]	1240	7600
Piezoelectric Constant, d_{33} [pC/N]	—	400×10^{-12}
Piezoelectric Constant, d_{31} [pC/N]	—	−175×10^{-12}
Piezoelectric Constant, d_{15} [pC/N]	—	590×10^{-12}
Relative Permittivity, $\varepsilon_{33}^{T}/\varepsilon_0$	—	1900

Table 2.

Simulation parameters for PZT arrangement selection study.

Simulation No.	Angle α_1	Angle α_2	Angle α_3	Simulation No.	Angle α_1	Angle α_2	Angle α_3
1	65	120	15	9	100	90	45
2	65	120	30	10	135	90	15
3	65	120	45	11	135	90	30
4	100	120	15	12	135	90	45
5	100	120	30	13	135	60	15
6	100	120	45	14	135	60	30
7	100	90	15	15	135	60	45
8	100	90	30				

Table 3.

Relative location of bearing and femoral components for the experiments.

Test No.	Relative location (mm)		Test No.	Relative location (mm)	
	x-direction	z-direction		x-direction	z-direction
Test 1	+3	0	Test 9	0	+4
Test 2	+2	0	Test 10	0	+3
Test 3	+1	0	Test 11	0	+2
Test 4	0	0	Test 12	0	+1
Test 5	−1	0	Test 13	0	0
Test 6	−2	0	Test 14	0	−1
Test 7	−3	0	Test 15	0	−2
Test 8	−4	0	Test 16	0	−3

Table 4.

Deviation of measured CP locations using PZTs from the true locations recorded by pressure films.

Test No.	Total Deviation (mm)		Test No.	Total Deviation (mm)	
	Medial compartment	Lateral compartment		Medial compartment	Lateral compartment
Test 1	0.8	0.9	Test 9	0.3	1.6
Test 2	1.3	1.2	Test 10	0.3	0.3
Test 3	1.4	1.2	Test 11	0.4	0.4
Test 4	0.6	0.7	Test 12	0.6	0.5
Test 5	0.5	0.4	Test 13	0.5	0.3
Test 6	0.3	0.3	Test 14	1.2	0.5
Test 7	1.4	1.3	Test 15	0.2	0.6
Test 8	0.7	1.3	Test 16	0.7	1.4